

# A Shock Tube Study of $\text{H} + \text{HNCO} \rightarrow \text{NH}_2 + \text{CO}$

JOHN D. MERTENS, KATHARINA KOHSE-HÖINGHAUS\*, RONALD K. HANSON, and CRAIG T. BOWMAN

*High Temperature Gasdynamics Laboratory, Department of Mechanical Engineering,  
Stanford University, Stanford, California 94305*

## Abstract

The reaction of atomic hydrogen with isocyanic acid (HNCO) to produce the amidogen radical ( $\text{NH}_2$ ) and carbon monoxide,



has been studied in shock-heated mixtures of HNCO dilute in argon. Time-histories of the ground-state  $\text{NH}_2$  radical were measured behind reflected shock waves using cw, narrow-linewidth laser absorption at 597 nm, and HNCO time-histories were measured using infrared emission from the fundamental  $\nu_2$ -band of HNCO near 5  $\mu\text{m}$ . The second-order rate coefficient of reaction (2(a)) was determined to be:

$$k_{2a} = 2.1 \times 10^{14} \exp(-8500/T, \text{K}) \quad (f = 0.5, F = 1.75) \quad T = 2340\text{--}3270 \text{ K},$$

$\text{cm}^3 \text{ mol}^{-1} \text{ s}^{-1}$ , where  $f$  and  $F$  define the lower and upper uncertainty limits, respectively.

An upper limit on the rate coefficient of

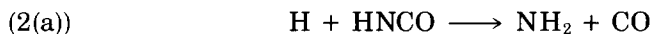


was determined to be:

$$k_5 \leq 5.0 \times 10^{11} \text{ cm}^3 \text{ mol}^{-1} \text{ s}^{-1}, \quad T = 2340\text{--}2680 \text{ K}.$$

## Introduction

The reaction of atomic hydrogen with isocyanic acid (HNCO) to produce the amidogen radical ( $\text{NH}_2$ ) and carbon monoxide,



plays an important role in the RAPRENO<sub>x</sub> process for NO reduction in combustion products [1]. Reaction (2(a)) also plays a role in fuel nitrogen conversion in rich flames [2]. The objective of the study reported in this article is to help refine current detailed kinetic models of these processes through the measurement of the rate coefficient of reaction (2(a)).

Reaction (2(a)) was studied in reflected shock wave experiments using initial mixture concentrations ranging from 0.5% to 2.0% HNCO dilute in argon. Time-histories of the  $\text{NH}_2$  radical were measured behind the shock waves using cw, narrow-linewidth laser absorption at 597 nm, while HNCO time-histories were measured using infrared emission from the fundamen-

\* On leave from DLR, Institut für Physikalische Chemie der Verbrennung, 7000 Stuttgart 80, Germany.

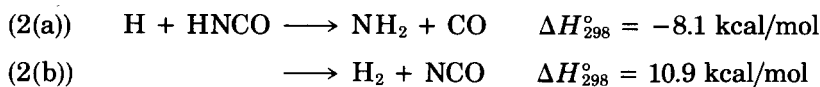
tal  $\nu_2$ -band of HNCO near  $5 \mu\text{m}$ . Over this range of initial HNCO mol-fractions, reaction (2(a)) becomes both the dominant  $\text{NH}_2$  formation reaction and the most important HNCO removal reaction. Hence, it is possible to make independent determinations of  $k_{2a}$  from the  $\text{NH}_2$  and the HNCO measurements.

For some experimental conditions,



becomes an important  $\text{NH}_2$ -removal reaction at early times. This makes it possible to determine an upper limit on  $k_5$  using the  $\text{NH}_2$  measurements.

To our knowledge, there have been no previous experimental studies of either reaction (2(a)) or reaction (5). Miller and Melius [3] have performed theoretical studies of the reaction of atomic hydrogen with HNCO based on fourth-order Moeller-Plesset perturbation theory with bond additivity corrections (BAC-MP4). They show that the reaction has two product channels:



Channel (2(b)) is relatively unimportant in the present study, and its impact on our results is discussed later in more detail.

### Experimental

The experimental apparatus comprises a shock tube and gas handling facility, a  $\text{NH}_2$  narrow-line laser diagnostic system, and an infrared emission detection system. A complete description of the shock tube and gas handling facility has been given previously [4].

The  $\text{NH}_2$  narrow-line laser diagnostic system has been described by Kohse-Höinghaus et al. [5]. In the present experiments,  $\text{NH}_2$  was monitored in the electronic ground-state using the  $\tilde{A}^2A_1 \leftarrow X^2B_1(090 \leftarrow 000)\Sigma^P Q_{1,N}(7)$  transition at 597.375 nm. This wavelength was obtained using a Spectra-Physics 380 ring dye laser with Rhodamine 590 dye pumped with 3-4 W (all-lines) from a Spectra-Physics model 171 argon ion laser. The wavelength and single-mode character of the dye laser beam were monitored using a Burleigh WA-10 wavemeter and a Spectra-Physics model 470 scanning interferometer. The dye laser power output was typically 30-35 mW. The beam was focused into the shock tube through  $\text{CaF}_2$  windows with a beam diameter of about 1.5 mm. A fraction of the beam was sampled before entering the shock tube to provide a reference beam. The reference and probe beams were monitored with amplified EG&G UV100B silicon photodiodes. The detector signals were balanced using neutral density filters to adjust the beam intensities. The probe and reference signals and the a.c.-coupled difference signal were recorded and stored on digital oscilloscopes (Nicolet model 2090) with  $0.5 \mu\text{s}$  sampling intervals. The temporal resolution of this system due to the spatial extent of the laser beam and the electronic response of the detectors was  $<4 \mu\text{s}$ .

The infrared emission detection system utilized a photo-voltaic InSb infrared detector (Judson Infrared Inc., 77 K,  $D_{\text{BB}}^* = 3.3 \times 10^{10} \text{ cm Hz}^{1/2}/\text{watt}$ ,  $1 \times 3 \text{ mm}$  active area) with matched pre-amplifier and a radiation col-

lection system to monitor emission from the fundamental  $\nu_2$ -band of HNCO near  $5 \mu\text{m}$ . A narrow-bandpass filter centered at  $4.5 \mu\text{m}$  with a FWHM of  $0.6 \mu\text{m}$  was mounted directly in front of the detector to minimize the collection of radiation from species other than HNCO. The a.c.-coupled output signal from the pre-amplifier was recorded and stored on a digital oscilloscope (Nicolet model 2090) with  $0.5 \mu\text{s}$  sampling intervals. The  $1/e$  electronic time response of this system was  $<1 \mu\text{s}$ . The radiation collection system comprised a  $\text{CaF}_2$  window, a flat turning mirror, an optical slit, and a 15 cm diameter spherical mirror with a nominal focal length of 30 cm. The system was configured and aligned using the focused-slit design and alignment procedure described in detail by Roose [6]. The important characteristic of this design is that the detector views a volume inside the shock tube that has a uniform width perpendicular to the shock front. This maximizes the radiation collected by the detector for a given spatial resolution. In the present study, the volume viewed by the detector had a width of about 2.5 mm.

All measurements were performed behind reflected shock waves. The infrared emission and  $\text{NH}_2$  absorption diagnostics were not used simultaneously. In the experiments utilizing the infrared emission diagnostic, a 10 cm wide strip centered about the test section window was painted black around the circumference of the inside of the shock tube in order to minimize the reflection of radiation originating from outside the volume viewed by the detector. The test section was not painted during the  $\text{NH}_2$  absorption experiments.

The HNCO was synthesized according to the procedure of Okabe [7]. Cyanuric acid,  $(\text{HOCN})_3$ , was heated in an evacuable Pyrex vessel above 250 C. The generated HNCO gas was solidified in a liquid nitrogen trap, then melted and vacuum distilled using a dry-ice/acetone trap ( $-78 \text{ C}$ ). The liquid HNCO was stored in a dry-ice/acetone bath for up to 5 days. Test mixtures were made by first adding HNCO vapor from the liquid HNCO to the evacuated mixing tank to pressures of 1 to 10 torr. Then argon was added to total pressures of 400 to 1500 torr to achieve the desired HNCO mol fractions. No evidence of adsorption was observed when the pressure of HNCO in the mixing tank was monitored over time. The purity of the HNCO vapor was found to be better than 98% by gas chromatography, with  $\text{CO}_2$  being the major impurity. The argon purity levels according to the manufacturer (Liquid Carbonic) were  $\geq 99.998\%$ .

## Results and Discussion

The measured species profiles were modeled with the reaction mechanism in Table I, using the Chemkin [8] and Senkin [9] computer programs and the Sandia National Laboratories thermodynamic data base [10]. The thermodynamic data base uses the following 298 K heats of formation in units of kcal/mol:  $\text{NH}$ : 85.2,  $\text{NH}_2$ : 45.5,  $\text{NCO}$ : 38.1,  $\text{HNCO}$ :  $-24.9$ . However, the calculations were not sensitive to small variations of these heats of formation. The reaction behind the reflected shock wave was modelled as a constant volume-constant internal energy process; over the time-scale of the experiments, temperature variations during reaction were negligible. The measured impurities in the HNCO were found to have no effect on the calculated  $\text{NH}_2$  and HNCO profiles when included in a more complicated re-

TABLE I. Reaction mechanism rate coefficients in form  $k_j = AT^B \exp(-\Theta/T)$  (units: mols, cc, s, and K).

	Reaction	log(A)	B	$\Theta$	(f, F) <sup>d</sup>	ref.
⇒	1a. HNCO + M = NH + CO + M	35.51	-5.11	55300.	(0.65, 1.50)	[4]
	1b. HNCO + M = H + NCO + M	15.70	0.0	60000.		<sup>a</sup>
⇒	2a. HNCO + H = NH <sub>2</sub> + CO	14.32	0.0	8500.		<sup>b</sup>
⇒	2b. HNCO + H = H <sub>2</sub> + NCO	7.02	2.0	8000.		[15]
	3. HNCO + N = NH + NCO	13.60	0.0	18000.		<sup>a</sup>
	4. HNCO + NH = NH <sub>2</sub> + NCO	13.30	0.0	12000.		<sup>a</sup>
⇒	5. HNCO + NH <sub>2</sub> = NH <sub>3</sub> + NCO	12.00	0.0	3500.		<sup>a</sup>
	6. NH + M = N + H + M	14.42	0.0	38000.		[4]
⇒	7. NH + H = N + H <sub>2</sub>	13.51	0.0	165.	(0.65, 1.35)	[12]
	8. NH + N = N <sub>2</sub> + H	11.80	0.5	0.		[14]
⇒	9. NH + NH = N <sub>2</sub> + H + H	13.71	0.0	0.	(0.7, 1.3)	[4]
⇒	10. NH + NH <sub>2</sub> = N <sub>2</sub> H <sub>2</sub> + H	15.18	-0.5	0.	(0.5, 1.5)	[12]
	11. NH <sub>2</sub> + M = NH + H + M	23.50	-2.0	46000.		[14]
⇒	12. NH <sub>2</sub> + H = NH + H <sub>2</sub>	13.60	0.0	1840.	(0.5, 1.5)	[12]
	13. NH <sub>2</sub> + N = N <sub>2</sub> + H + H	13.86	0.0	0.		[2]
	14. NH <sub>2</sub> + NH <sub>2</sub> = NH <sub>3</sub> + NH	13.70	0.0	5000.		[12]
	15. NH <sub>2</sub> + NH <sub>2</sub> = N <sub>2</sub> H <sub>2</sub> + H <sub>2</sub>	13.60	0.0	6000.		[14]
	16. NH <sub>3</sub> + M = NH <sub>2</sub> + H + M	16.34	0.0	47030.		[12]
	17. NH <sub>3</sub> + M = NH + H <sub>2</sub> + M	14.80	0.0	47000.		[14]
	18. NH <sub>3</sub> + H = NH <sub>2</sub> + H <sub>2</sub>	5.81	2.39	5120.		[2]
	19. NH <sub>3</sub> + NH <sub>2</sub> = N <sub>2</sub> H <sub>3</sub> + H <sub>2</sub>	11.90	0.5	10850.		[14]
	20. H + H + M = H <sub>2</sub> + M	18.00	-1.0	0.		[2]
	H <sub>2</sub> /0/H <sub>2</sub> O/0/ <sup>c</sup>					
	21. H + H + H <sub>2</sub> = H <sub>2</sub> + H <sub>2</sub>	16.96	-0.6	0.		[2]
	22. N <sub>2</sub> + M = N + N + M	20.87	-1.6	113200.		[14]
	N <sub>2</sub> /5.0/ <sup>c</sup>					
	23. NNH + M = N <sub>2</sub> + H + M	14.00	0.0	1500.		<sup>a</sup>
	24. NNH + H = N <sub>2</sub> + H <sub>2</sub>	13.60	0.0	1500.		[14]
	25. NNH + N = NH + N <sub>2</sub>	13.50	0.0	1000.		[14]
	26. NNH + NH = N <sub>2</sub> + NH <sub>2</sub>	11.30	0.5	1000.		[14]
	27. NNH + NH <sub>2</sub> = N <sub>2</sub> + NH <sub>3</sub>	13.00	0.0	0.		[14]
	28. N <sub>2</sub> H <sub>2</sub> + M = NNH + H + M	16.00	0.0	25000.		[14]
	29. N <sub>2</sub> H <sub>2</sub> + M = NH + NH + M	16.50	0.0	50000.		[14]
	30. N <sub>2</sub> H <sub>2</sub> + H = NNH + H <sub>2</sub>	13.00	0.0	500.		[14]
	31. N <sub>2</sub> H <sub>2</sub> + NH = NNH + NH <sub>2</sub>	13.00	0.0	500.		[14]
	32. N <sub>2</sub> H <sub>2</sub> + NH <sub>2</sub> = NNH + NH <sub>3</sub>	13.00	0.0	2000.		[14]
	33. N <sub>2</sub> H <sub>3</sub> + M = N <sub>2</sub> H <sub>2</sub> + H + M	16.00	0.0	25000.		[14]
	34. N <sub>2</sub> H <sub>3</sub> + M = NH <sub>2</sub> + NH + M	16.00	0.0	21000.		[14]
	35. N <sub>2</sub> H <sub>3</sub> + H = NH <sub>2</sub> + NH <sub>2</sub>	12.20	0.0	0.		[14]
	36. N <sub>2</sub> H <sub>3</sub> + H = NH + NH <sub>3</sub>	11.00	0.0	0.		[14]
	37. N <sub>2</sub> H <sub>3</sub> + H = N <sub>2</sub> H <sub>2</sub> + H <sub>2</sub>	12.00	0.0	1000.		[14]
	38. NCO + M = N + CO + M	22.10	-2.0	33600.		[16]
	39. NCO + H = NH + CO	13.70	0.0	0.		[2]
	40. NCO + N = N <sub>2</sub> + CO	13.30	0.0	0.		[2]
	41. HCO + M = CO + H + M	14.40	0.0	8456.		[2]
	CO/1.9/H <sub>2</sub> /1.9/CO <sub>2</sub> /3.0/H <sub>2</sub> O/5.0/ <sup>c</sup>					
	42. HCO + H = CO + H <sub>2</sub>	13.08	0.25	0.		[2]

<sup>a</sup> Estimate.<sup>b</sup> This work.<sup>c</sup> Enhanced third-body efficiencies.<sup>d</sup> Uncertainty limits used in uncertainty analysis for  $k_{2a}$ . ⇒ Reactions important in this study.

action mechanism [11], and they were subsequently neglected in the calculations. In addition to calculating species concentration profiles, the computer programs were used to calculate reaction contribution factors and sensitivity coefficients. A reaction contribution factor is the net rate of production or destruction of a particular species by a particular reaction. For example, the  $\text{NH}_2$  contribution factor for reaction (2(a)) is:

$$R_{2a}(t) = k_{2a}(\text{HNCO})(\text{H}) - k_{-2a}(\text{NH}_2)(\text{CO}) \text{ molcm}^{-3} \text{ s}^{-1}$$

The sensitivity coefficient,  $\alpha_{ij}$ , calculated by Senkin, is the partial derivative of the molfraction of a species  $j$ ,  $X_j$ , with respect to the temperature independent rate constant parameter  $A_i$  of a reaction  $i$ , normalized by the maximum species molfraction and the rate constant parameter  $A_i$ :

$$\alpha_{ij}(t) = (A_i/X_j^{\text{max}})(\partial X_j/\partial A_i)$$

### *NH<sub>2</sub> Absorption Measurements*

The test conditions and results of the  $\text{NH}_2$  measurements are given in Table II. Two initial mixture concentrations were used: 0.6% HNCO and 2.0% HNCO dilute in argon. Reflected shock temperatures and pressures ranged from 2340 to 3260 K and 0.34 to 0.49 atmospheres, respectively. Gas properties were assumed to be uniform in the plane parallel to the shock front. The peak  $\text{NH}_2$  concentrations ranged from 220 ppm to 1000 ppm, with the detection limits (SNR = 1) varying from 20 ppm to 100 ppm. A typical measured  $\text{NH}_2$  absorption profile is shown in Figure 1. The sharp peaks at  $-55 \mu\text{s}$  and time zero are the consequence of shock-front-induced beam steering by the incident and reflected shock waves. The fractional absorption profiles were converted into molfractions using the Beer-Lambert law and  $\text{NH}_2$  absorption coefficients measured by Kohse-Höinghaus et al. [5] and Davidson et al. [12]. In these two studies, the absorption coefficients were determined by matching predicted  $\text{NH}_2$  concentrations to measured  $\text{NH}_2$  absorption levels in ammonia pyrolysis and photolysis shock tube experiments. The more recent determination of Davidson et al. is given by the

TABLE II. Conditions and results for  $k_{2a}$  from  $\text{NH}_2$  absorption measurements.

Temperature (K)	Total pressure (atm)	Initial HNCO mol fraction (%)	$k_{2a} \times 10^{-13}$ ( $\text{cm}^3 \text{ mol}^{-1} \text{ s}^{-1}$ )
3262	0.339	1.950	1.35
3167	0.355	1.950	1.35
3050	0.369	1.950	1.05
2804	0.400	1.950	0.80
2684	0.427	1.950	0.83
2526	0.461	1.950	0.70
2338	0.492	1.950	0.50
3219	0.342	0.585	1.60
2994	0.390	0.585	1.10
2949	0.391	0.585	1.25
2790	0.412	0.585	0.95
2628	0.433	0.585	0.70

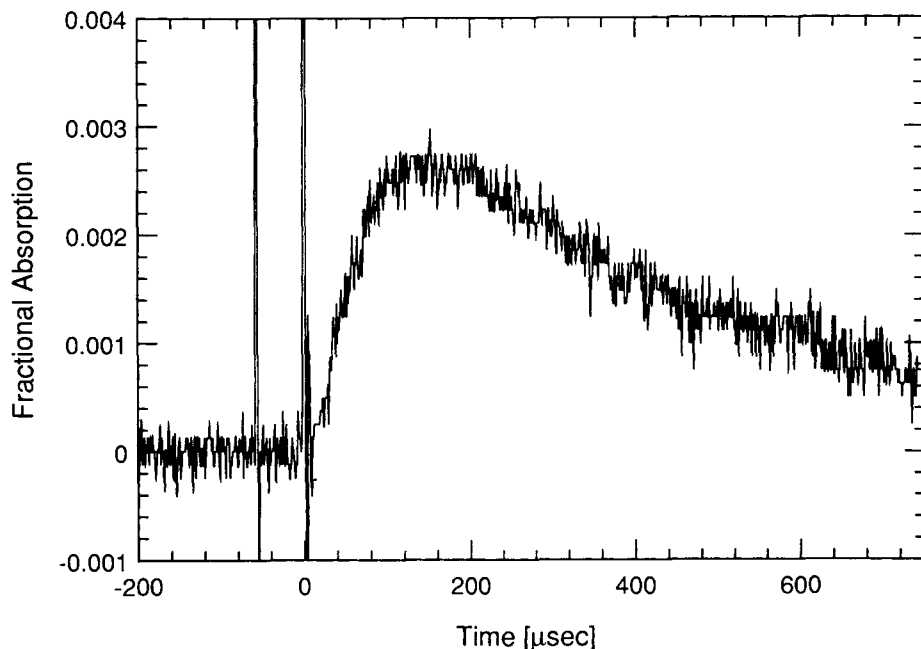


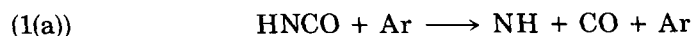
Figure 1. Typical measured  $\text{NH}_2$  fractional absorption profile in a reflected shock wave experiment. Peak absorption corresponds to 270 ppm  $\text{NH}_2$ , 0.6%  $\text{HNCO}$  in argon,  $T = 2628$  K, and  $P = 0.433$  atm.

expression:

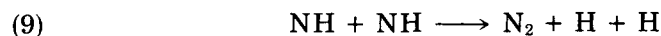
$$k_{\text{NH}_2}(\text{abs. coef.}) = 4.319 \times 10^{10}/T^3 + 7.969 \times 10^5/T^2 - 1.693 \\ \times 10^3/T \text{ atm}^{-1} \text{ cm}^{-1},$$

where  $T$  is in degrees K. This result is valid for total pressures on the order of 1 atmosphere, with an overall uncertainty of  $\pm 30\%$ .

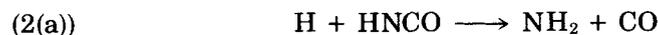
*Reaction (2a)*:  $\text{NH}_2$  is produced in shock-heated mixtures of  $\text{HNCO}$  dilute in argon through a series of reactions. The initial step is the dissociation of  $\text{HNCO}$  to produce  $\text{NH}$ :



This reaction is followed by the production of H-atoms by the fast reaction:



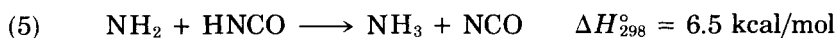
The H-atoms then react with  $\text{HNCO}$  to generate  $\text{NH}_2$ :



As the radical pool increases, and the  $\text{HNCO}$  concentration decreases, reactions of  $\text{NH}_2$  with other species eventually overcome the  $\text{NH}_2$  production, and the  $\text{NH}_2$  profile reaches a peak and begins to decay. However, the calculated  $\text{NH}_2$  profile is sensitive primarily to the rate coefficients of reactions (1(a)) and (2(a)). The second-order rate coefficients of reactions (1(a)) and (9) [4] and several other contributing reactions [4,12] were recently measured in this laboratory. This makes it possible to determine the rate

coefficient of reaction (2(a)) by adjusting  $k_{2a}$  in the reaction mechanism until the calculated  $\text{NH}_2$  profiles fit the data. Figure 2 shows a typical fit to the data, as well as the effect of a  $\pm 20\%$  adjustment in  $k_{2a}$  which clearly exceeds the uncertainty associated with the noise of the trace. The total uncertainty of the determination of  $k_{2a}$  is discussed below. Figure 3 is a reaction contribution factor plot for  $\text{NH}_2$  for the same experiment that shows that reaction (2(a)) is the dominant  $\text{NH}_2$  reaction. Figure 4 is a sensitivity coefficient plot for  $\text{NH}_2$  for the same experiment, showing that the  $\text{NH}_2$  profile is somewhat sensitive to the rate coefficients of several reactions that do not directly involve  $\text{NH}_2$ . These reactions contribute to the production and removal of H-atoms, and the uncertainties in the rate coefficients of these reactions, given in Table I, were included in the uncertainty analysis. Figure 5 is an Arrhenius plot that includes the results of the  $\text{NH}_2$  measurements and the HNCO measurements discussed later. The typical uncertainty limits shown on Figure 5 for several individual  $\text{NH}_2$  measurements were determined using dependent and independent error propagation analysis [13]. They represent the combined effects of the  $\pm 30\%$  uncertainty of the  $\text{NH}_2$  absorption coefficient, the noise of the data traces, and the uncertainties of the rate coefficients of other reactions.

*Reaction (5):* For three of the lower-temperature ( $T = 2340\text{--}2680\text{ K}$ ), higher-initial HNCO concentration (2.0% HNCO) experiments, reaction (5):



becomes an important  $\text{NH}_2$ -removal reaction at early times. Although reaction (2(a)) still is the most important  $\text{NH}_2$  reaction, it is not possible to

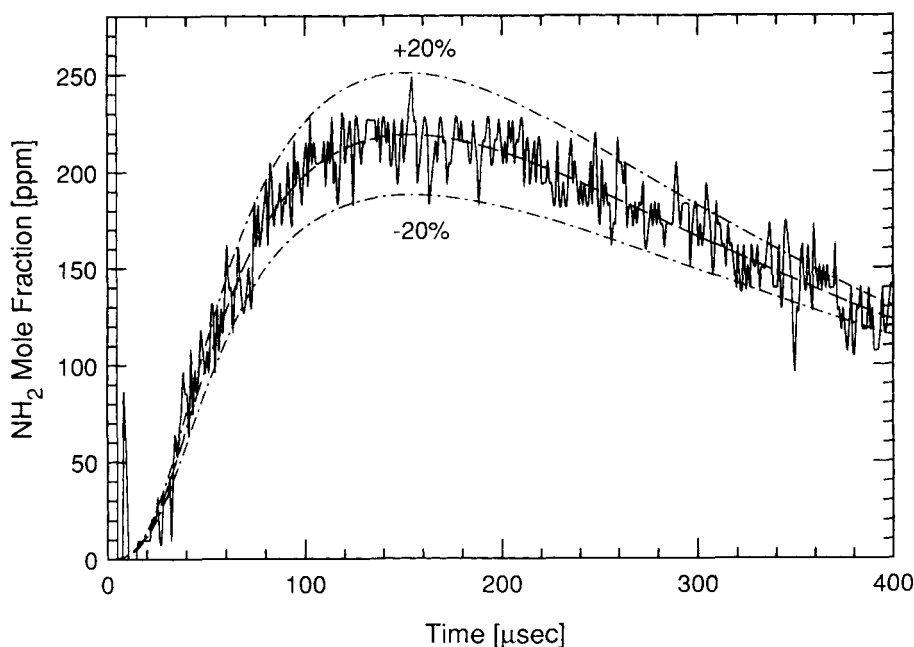


Figure 2. Determination of  $k_{2a}$  from a fit of the reduced data of Figure 1. Dashed lines:  $k_{2a} = 7.0 \times 10^{12} \text{ cm}^3 \text{ mol}^{-1} \text{ s}^{-1}$  with  $\pm 20\%$  variation.

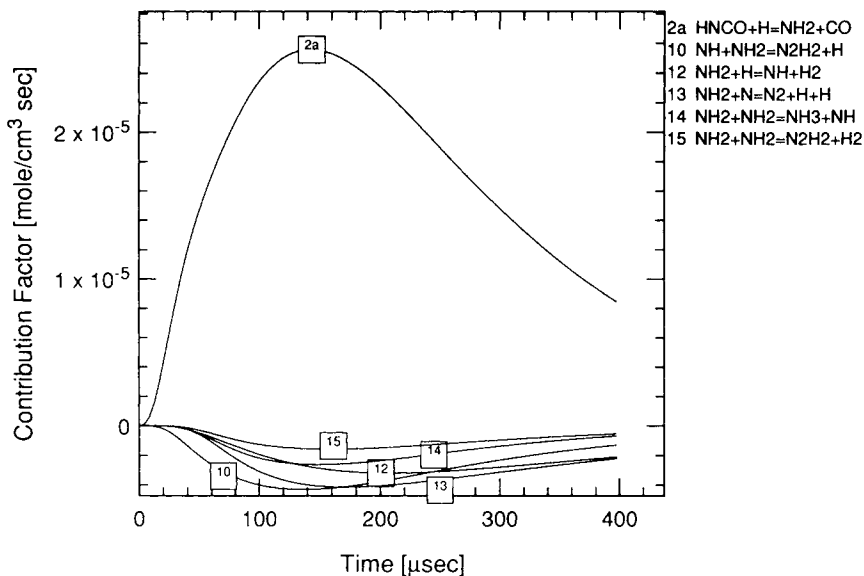


Figure 3. Calculated  $\text{NH}_2$  reaction contribution factor plot for the conditions of Figure 2.

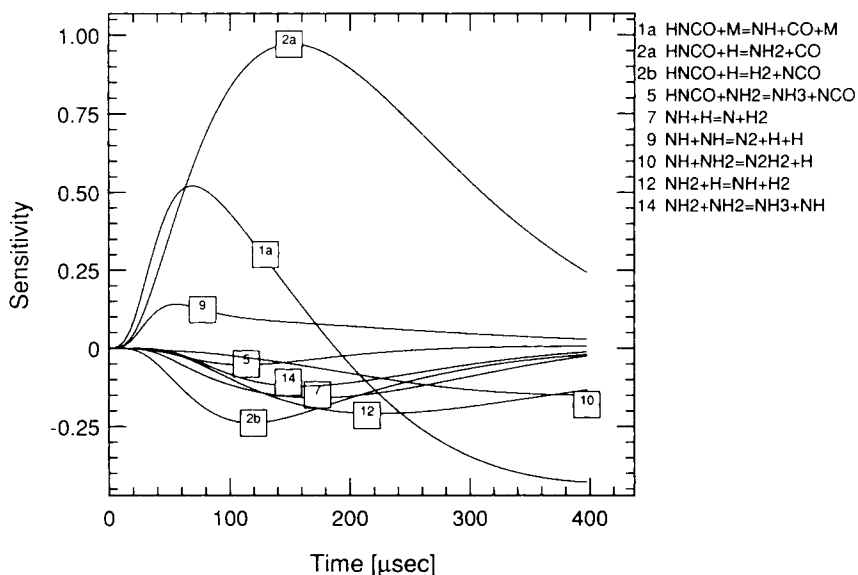


Figure 4. Calculated  $\text{NH}_2$  sensitivity coefficient plot for the conditions of Figure 2.

fit the measured  $\text{NH}_2$  profiles at early times while remaining within acceptable uncertainty limits of other rate parameters if the value of  $k_5$  is raised above an upper limit. The upper limits of  $k_5$  determined from the three experiments are:

$$k_5 \leq 4.0 \times 10^{11} \text{ cm}^3 \text{ mol}^{-1} \text{ s}^{-1}, \quad T = 2340 \text{ K},$$

$$k_5 \leq 5.0 \times 10^{11} \text{ cm}^3 \text{ mol}^{-1} \text{ s}^{-1}, \quad T = 2530 \text{ K},$$

$$k_5 \leq 5.0 \times 10^{11} \text{ cm}^3 \text{ mol}^{-1} \text{ s}^{-1}, \quad T = 2680 \text{ K}.$$

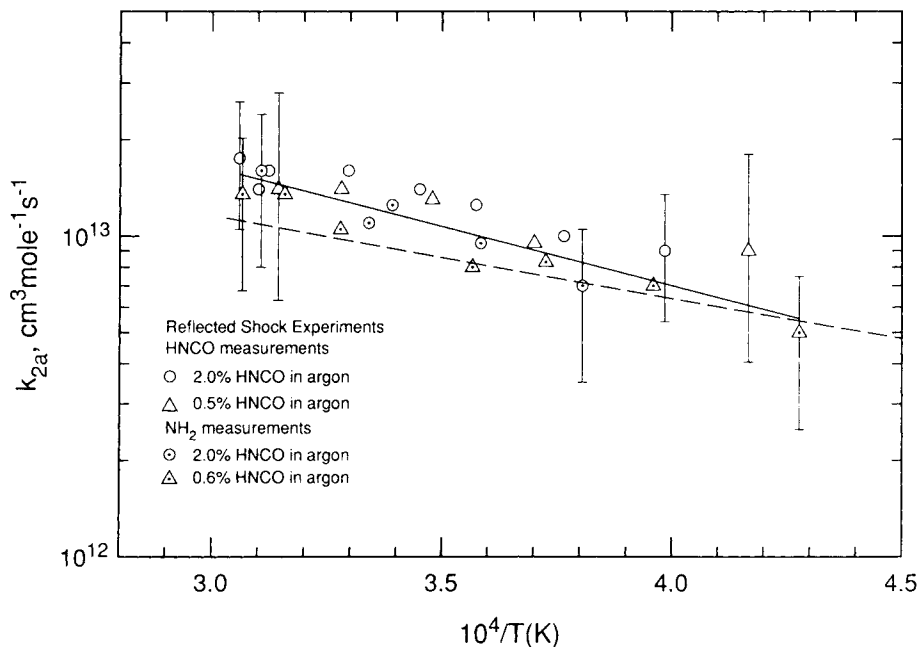


Figure 5. Arrhenius diagram for reaction (2(a)). Solid line: two-parameter least-squares fit using individual point uncertainties of the results of  $\text{NH}_2$  and HNCO measurements and  $k_{2a} = 2.1 \times 10^{14} \exp(-8500/T, \text{K}) \text{ cm}^3 \text{ mol}^{-1} \text{ s}^{-1}$ . Dashed line: calculations of Miller and Melius [3].

### *HNCO Infrared Emission Measurements*

The test conditions and results of the HNCO measurements are given in Table III. Two initial mixture concentrations were used: 0.5% HNCO and 2.0% HNCO dilute in argon. Reflected shock temperatures and pressures ranged from 2400 to 3270 K and 0.27 to 0.77 atmospheres, respectively.

A typical infrared emission profile is shown in Figure 6. The first rise to a plateau at  $-55 \mu\text{s}$  corresponds to the heating of the test gas by the arrival

TABLE III. Conditions and results for  $k_{2a}$  from infrared emission measurements.

Temperature (K)	Total pressure (atm)	Initial HNCO mol fraction (%)	$k_{2a} \times 10^{-13}$ ( $\text{cm}^3 \text{ mol}^{-1} \text{ s}^{-1}$ )
3269	0.270	2.001	1.75
3225	0.770	2.001	1.4
3202	0.306	2.001	1.6
3034	0.337	2.001	1.6
2898	0.348	2.001	1.4
2798	0.368	2.001	1.25
2656	0.399	2.001	1.0
2510	0.412	2.001	0.9
3181	0.329	0.500	1.4
3048	0.353	0.500	1.4
2875	0.374	0.500	1.3
2702	0.398	0.500	0.95
2400	0.472	0.500	0.9

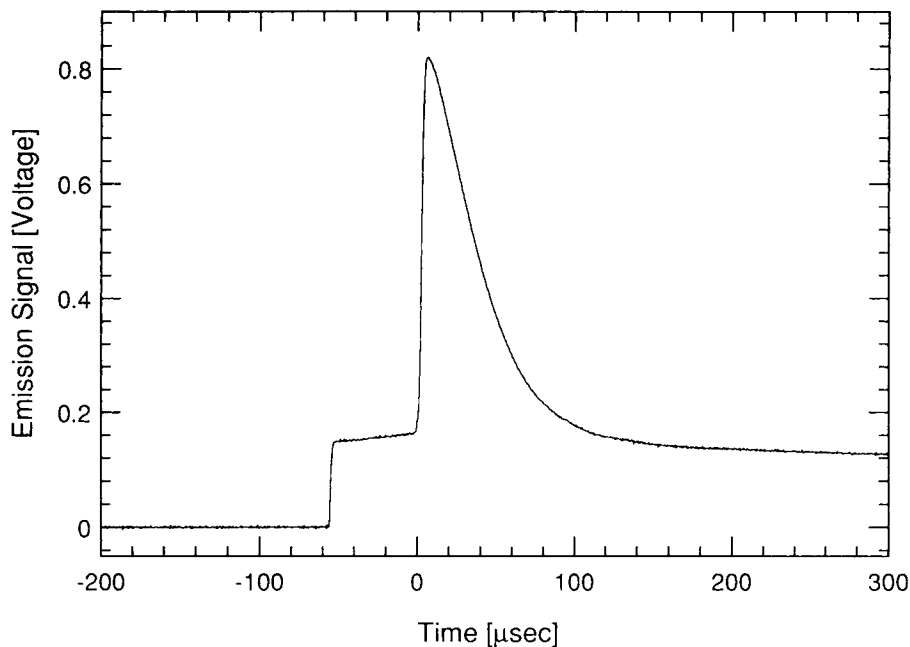


Figure 6. Typical measured HNCO infrared emission profile in a reflected shock wave experiment. 2.0% HNCO in argon,  $T = 3034$ , K, and  $P = 0.337$  atm.

of the incident shock wave. The incident shock temperatures were not high enough to initiate reaction. The slight rise in this plateau is due to radiation that originated from behind the approaching reflected shock wave, and was reflected off of the shock tube walls into the solid angle viewed by the detector. The second rise to a maximum at time zero is due to the heating of the test gas by the arrival of the reflected shock wave. The rise time to the peak is approximately  $5 \mu\text{s}$ , which corresponds to the reflected shock wave transit time across the  $2.5 \text{ mm}$  width of the volume viewed by the detector. The subsequent decrease of the signal corresponds to the decomposition of HNCO. The emission signal does not reach zero at long times because of background emission near  $5 \mu\text{m}$  from CO formed during HNCO decomposition.

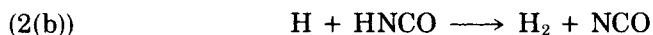
*Reaction (2a):* In shock tube experiments with high initial HNCO mol-fractions (HNCO > 0.1%), reaction (2a) becomes an important, and for some conditions, the most important HNCO-removal channel. This makes it possible to make an additional determination of  $k_{2a}$ , independent of the  $\text{NH}_2$  measurements, by adjusting  $k_{2a}$  until calculated HNCO emission profiles fit the measured emission traces. However, before calculated HNCO emission profiles can be compared to the data, they must be corrected for the non-ideal features of the measurements.

First, the interference radiation from CO must be accounted for. In order to calculate a combined HNCO/CO emission profile, both the HNCO and CO mol-fraction profiles are calculated using the reaction mechanism in Table I. The calculated CO profile is then multiplied by the ratio of the emission signal of one CO molecule to the emission signal of one HNCO molecule at the reflected shock temperature. These values were determined from the shock-heated HNCO peak emission values and similar tests using CO mixtures in argon. This ratio, measured for this particular infrared sys-

tem and filter, was a nearly linear function of temperature, with a value of 0.175 at 3300 K and 0.14 at 2400 K. The calculated CO emission profile then is added to the calculated HNCO molfraction profile to simulate the measured emission profile. Since CO is chemically inert in this environment, and one CO molecule is produced for each HNCO molecule that is removed, the CO profile is essentially a mirror image of the HNCO profile. Hence, the combined HNCO/CO profile is sensitive only to the HNCO profile.

The second nonideal feature of the measured emission profile is the time averaging of the signal due to the finite width of the volume viewed by the detector. This is dealt with by convolving the combined HNCO/CO calculated profile with the measured shock wave transit function. The result is normalized such that the peak value is unity and compared to the measured emission profile, which is normalized in the same fashion.

HNCO profiles determined in this manner were fit to the measured profiles by adjusting  $k_{2a}$  in the reaction mechanism. Figure 7 shows a typical fit to the data, as well as the effect of a  $\pm 30\%$  adjustment of  $k_{2a}$ . Figure 8 is a reaction contribution factor plot for HNCO for the same experiment. This plot shows that reaction (1(a)) and reaction (2(b)),



are the only other significant HNCO reactions. Figure 9 is a sensitivity coefficient plot for HNCO for the same experiment. These plots show that, although reaction (2(b)) contributes to the removal of HNCO, the HNCO profile is only slightly sensitive to changes in  $k_{2b}$ . Figure 9 also shows that the HNCO profile is somewhat sensitive to the rate coefficients of several

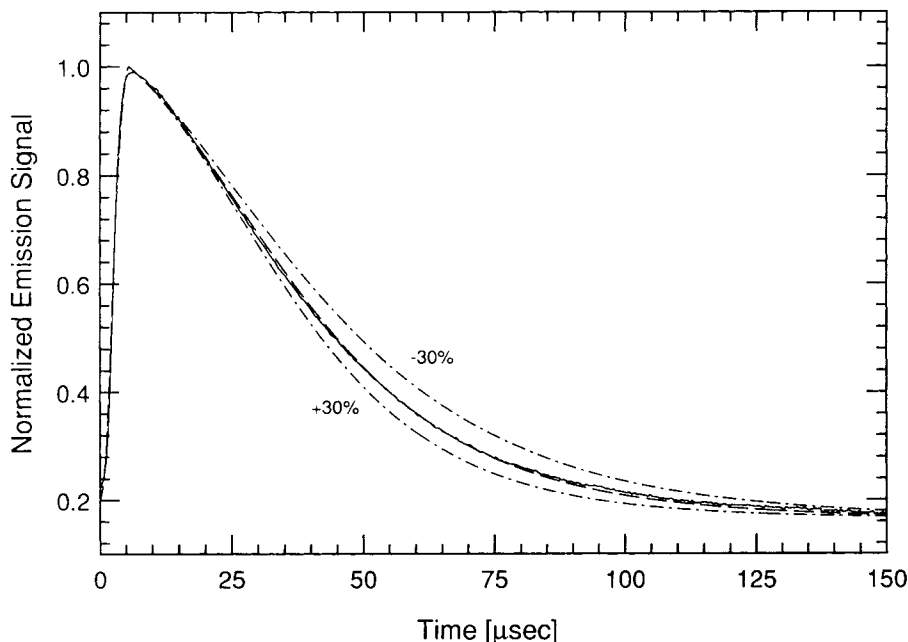


Figure 7. Determination of  $k_{2a}$  from a fit of the normalized emission profile of Figure 6. Dashed lines:  $k_{2a} = 1.6 \times 10^{13} \text{ cm}^3 \text{ mol}^{-1} \text{ s}^{-1}$  with  $\pm 30\%$  variation.

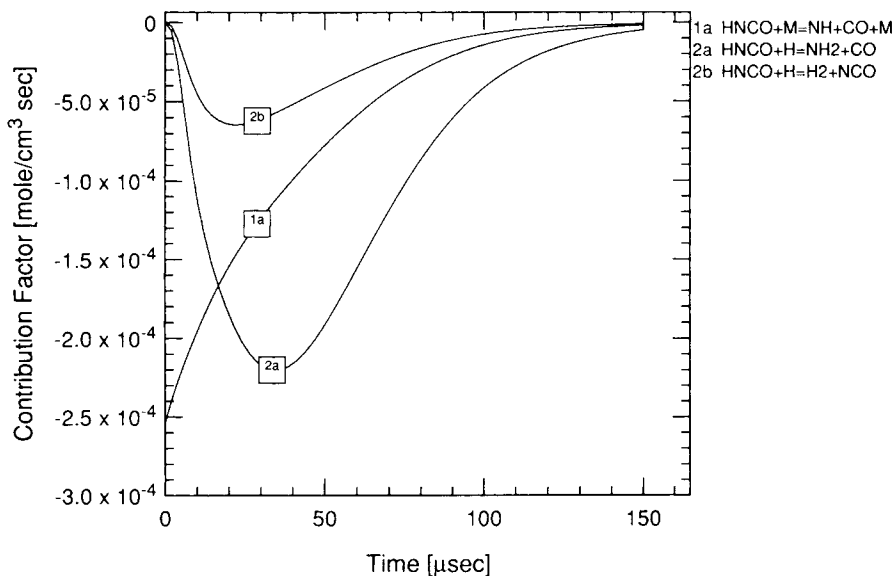


Figure 8. Calculated HNCO reaction contribution factor plot for the conditions of Figure 7.

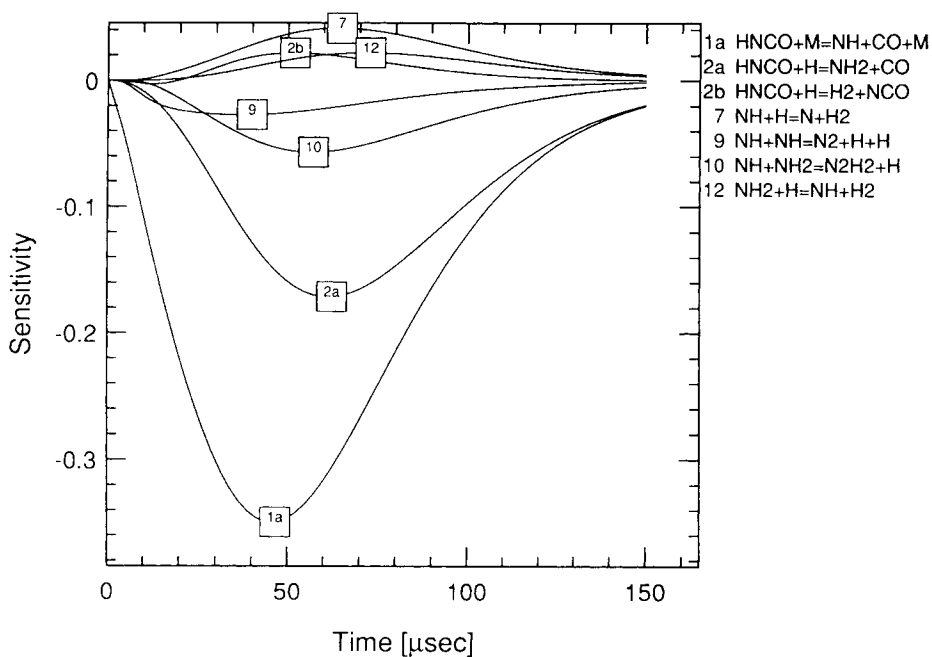


Figure 9. Calculated HNCO sensitivity coefficient plot for the conditions of Figure 7.

reactions that do not directly involve HNCO. These reactions contribute to the production and removal of H-atoms, and the uncertainties in the rate coefficients of these reactions, shown in Table I, were included in the uncertainty analysis.

The Arrhenius plot of Figure 5 shows that there is good agreement between the independent results of the  $\text{NH}_2$  and HNCO measurements. The

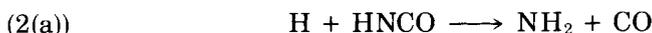
typical uncertainty limits shown on Figure 5 for several individual HNCO measurements were determined using dependent and independent error propagation analysis [13]. They represent the combined effects of the uncertainty of fitting the measured emission profiles and the uncertainties of the rate coefficients of other reactions. A least-squares two-parameter fit of the results of both the  $\text{NH}_2$  and HNCO measurements, using individual point uncertainties, is given by:

$$k_{2a} = 2.1 \times 10^{14} \exp(-8500/T, \text{K}) \text{ cm}^3 \text{ mol}^{-1} \text{ s}^{-1} \quad (f = 0.5, F = 1.75).$$

The minimum and maximum rate coefficient factors [14] ( $f, F$ ) represent the combined effects of the uncertainties of both the  $\text{NH}_2$  and HNCO measurements; i.e.,  $fk_{2a}$  and  $Fk_{2a}$  give the minimum and maximum possible values of  $k_{2a}$  determined by the uncertainty analysis. The activation energy of the above expression for  $k_{2a}$  is a parameter determined by the least-squares fitting procedure and is subject to large uncertainties. However, both the experimental data and the theoretical results of Miller and Melius [3] suggest that reaction (2(a)) has a small positive temperature dependence. Figure 5 shows good agreement between the theoretical  $k_{2a}$ -values of Miller and Melius and the results of the present study. We have found no previous experimental determinations of the rate coefficient of reaction (2(a)).

### Conclusion

The second-order rate coefficient of the reaction:

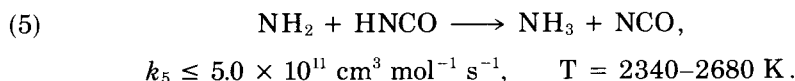


was determined to be:

$$k_{2a} = 2.1 \times 10^{14} \exp(-8500/T, \text{K}) \quad (f = 0.5, F = 1.75) \quad T = 2340\text{--}3270 \text{ K}$$

$\text{cm}^3 \text{ mol}^{-1} \text{ s}^{-1}$ , using both  $\text{NH}_2$  and HNCO measurements in the shock wave pyrolysis of HNCO. This result helps refine current detailed kinetics models of combustion processes such as RAPRENO<sub>x</sub> and fuel nitrogen conversion in flames.

$\text{NH}_2$  measurements also resulted in the determination of an upper limit on the rate coefficient of reaction (5):



### Acknowledgments

This work was supported by the Environmental Protection Agency and the Air Force Office of Scientific Research.

### Bibliography

- [1] J. A. Miller and C. T. Bowman, *Int. J. Chem. Kinet.*, **23**, 289 (1991).
- [2] J. A. Miller and C. T. Bowman, *Prog. in Energy and Combust. Sci.*, **15**, 287 (1989).
- [3] J. A. Miller and C. F. Melius, in preparation.
- [4] J. D. Mertens, A. Y. Chang, R. K. Hanson, and C. T. Bowman, *Int. J. Chem. Kinet.*, **21**, 1049 (1989).

- [5] K. Kohse-Höinghaus, D. F. Davidson, and R. K. Hanson, *J. Quant. Spectrosc. Radiat. Transfer*, **42**, 1 (1989).
- [6] T. R. Roose, *Ph.D. Thesis*, Stanford University, 1981.
- [7] H. Okabe, *J. Chem. Phys.*, **53**, 3507 (1970).
- [8] R. J. Kee, J. A. Miller, and T. H. Jefferson, *Chemkin: A General-Purpose Problem-Independent, Transportable, Fortran Chemical Kinetics Code Package*, Sandia National Laboratory Report No. SAND80-8003, 1980.
- [9] A. E. Lutz, R. J. Kee, and J. A. Miller, *Senkin: A Fortran Program for Predicting Homogeneous Gas Phase Chemical Kinetics with Sensitivity Analysis*, Sandia National Laboratory Report No. SAND87-8248, 1988.
- [10] R. J. Kee, F. M. Rupley, and J. A. Miller, *The Chemkin Thermodynamic Data Base*, Sandia National Laboratory Report No. SAND87-8215, 1987.
- [11] J. D. Mertens, A. Y. Chang, R. K. Hanson, and C. T. Bowman, *Int. J. Chem. Kinet.*, **23**, 173 (1991).
- [12] D. F. Davidson, K. Kohse-Höinghaus, A. Y. Chang, and R. K. Hanson, *Int. J. Chem. Kinet.*, **22**, 513 (1990).
- [13] S. L. Meyer, *Data Analysis for Scientists and Engineers*, Wiley, 1975.
- [14] R. K. Hanson and S. Salimian, *Combustion Chemistry*, W.C. Gardiner, Jr., Ed., Springer-Verlag, 1984, Chap. 6.
- [15] J. A. Miller, private communication, 1989.
- [16] J. D. Mertens, A. J. Dean, R. K. Hanson, and C. T. Bowman, in preparation.

Received October 12, 1990

Accepted January 23, 1991